Acta Cryst. (1977). A33, 784–788

Electron Diffraction Study of Short-Range-Order Diffuse Scattering from Disordered Binary Alloys

BY KEN-ICHI OHSHIMA* AND DENJIRO WATANABE

Department of Physics, Tohoku University, Sendai, Japan

(*Received* 13 *December* 1976; *accepted* 17 *March* 1977)

A qualitative study was made by electron diffraction of the short-range-order diffuse scattering from disordered Au–Pd, α phase Au–Zn, and α phase Ag–Mg alloys. Twofold and fourfold splittings of diffuse maxima are observed at 100, 110 and equivalent positions on the diffraction patterns with the incident beam parallel to [001], in the composition ranges from about 28 to 62 at.% Pd for Au–Pd, from about 7 to 24 at.% Zn for Au–Zn and from about 11 to 28 at.% Mg for Ag–Mg systems. The separation of the split diffuse maxima increases monotonically with Pd, Zn or Mg content. The results can be interpreted with the Fermi-surface-imaging concept proposed by Krivoglaz. The variation with composition of the Fermi wave vector parallel to the [110] directions is discussed with the nearly-free-electron and the rigid-band models. The latter model is also applied to the experimental results for disordered Cu–Pd and Cu–Pt alloys reported by the present authors [Ohshima & Watanabe (1973), *Acta Cryst.* A**29**, 520–526].

I. Introduction

Diffraction patterns from some disordered alloys exhibit peculiar diffuse scattering due to short-range order (SRO). In particular, for alloys of Cu–Au (Raether, 1952; Sato, Watanabe & Ogawa, 1962; Watanabe & Fisher, 1965; Hashimoto & Ogawa, 1970), Cu-rich Cu–Al (Scattergood, Moss & Bever, 1970), Cu–Pd (Watanabe, 1959; Ohshima & Watanabe, 1973; Ohshima, Watanabe & Harada, 1976), Cu–Pt (Ohshima & Watanabe, 1973), and Au–40·0 at.% Pd (Lin, Spruiel & Williams, 1970), which have a face-centred cubic (f.c.c.) structure above the order–disorder transformation temperature T_c, twofold and fourfold splittings of diffuse maxima have been observed at 100, 110, and equivalent positions on the net of the reciprocal lattice containing $hk0$ reflexions. The separation of the split diffuse maxima scarcely changes with composition for the Cu–Au system, but it increases monotonically with increase in the concentration of the alloying element for the Cu-rich Cu–Al, Cu–Pd, and Cu–Pt alloys. These results can be well understood from the Fermi-surface-imaging concept proposed by Krivoglaz (1969).

It is very difficult to study the Fermi surface of disordered binary alloys because of the short mean free path of the conduction electrons, and there are only a few procedures for investigating it. Observation of the SRO diffuse scattering by the electron diffraction method is very suitable for this study because it is easy to prepare samples. Therefore, it should be worthwhile investigating a number of disordered alloys by electron diffraction.

In the present study, the composition dependence of the diffuse scattering distribution is investigated by electron diffraction for the disordered Au–Pd, α phase Au–Zn, and α phase Ag–Mg alloys, and a relation between the SRO diffuse scattering and the Fermi surface of these alloys is discussed using the nearly-free-electron and the rigid-band models. The experimental results for disordered Cu–Pd and Cu–Pt alloys previously reported [Ohshima & Watanabe, 1973 (hereinafter referred to as part I)] are re-examined with the rigid-band model.

The Au–Pd alloy system forms a continuous series of f.c.c. solid solutions (Hansen & Anderko, 1958). By electron diffraction from thin evaporated films, Nagasawa, Matsuo & Kakinoki (1965) and Matsuo, Nagasawa & Kakinoki (1966) discovered the existence of an $L1_2$-type superstructure in the compositions near Au_3Pd and $AuPd_3$. However, Kawasaki, Ino & Ogawa (1971) confirmed that a superstructure was formed only in the composition near $AuPd_3$. The short-range order was studied by Copeland & Nicholson (1964) for an alloy with 40 at.% Pd and by Iveronova & Katsnel'son (1965, 1966) for alloys with 40, 50 and 60 at.% Pd, with X-ray powder diffraction methods. A single-crystal X-ray study was made by Lin *et al.* (1970) for 40·0 at.% Pd alloy, and the result was explained with the Fermi-surface-imaging concept by Cowley & Wilkins (1972). However, characteristic diffuse streaks, the intersections of which correspond to the split diffuse maxima, were not detected in the X-ray study, and the composition dependence of the separation of the split maxima has not been examined yet.

At elevated temperatures the α phase Au–Zn and Ag–Mg alloys form f.c.c. solid solutions up to compositions of 31 at.% Zn and 28 at.% Mg respectively (Hansen & Anderko, 1958). In the Au–Zn system, the complex ordered structures with a long period exist below T_c (Schubert, Kiefer, Wilkens & Haufler, 1955; Iwasaki, Hirabayashi, Watanabe & Ogawa, 1960; Iwasaki, 1962). In the Ag–Mg system, a periodic one-dimensional anti-phase domain structure based on a face-centred tetragonal cell with an atomic arrangement of the ordered Cu_3Au type appears in the composition range of 20 to 28 at.% Mg (Schubert *et al.*,

* Present address: Department of Applied Physics, Nagoya University, Nagoya, Japan.

1955; Fujiwara, Hirabayashi, Watanabe & Ogawa, 1958; Hanhi, Mäki & Paalassalo, 1971). No study of the SRO diffuse scattering has yet been reported, however.

II. Experimental

Bulk specimens were prepared within an atmosphere of purified argon in a plasma-jet arc furnace for Au–Pd alloys and in a silica tube for Au–Zn and Ag–Mg alloys. Purity of the starting materials was 99·99% for Au and 99·9% for the others. The Au–Pd alloys were homogenized by vacuum annealing for 5 d at 1000 °C, the Au–Zn alloys in a silica tube filled with argon for 7 d at 600 °C, and the Ag–Mg alloys in a graphite crucible inside a silica tube filled with argon for 7 d at 650 °C. The specimens were rolled into thin sheets 0·1 ~ 0·2 mm thick, annealed at various temperatures above T_c and quenched in ice brine.

Lattice parameters of the quenched specimens in the disordered state were measured with a Debye–Scherrer X-ray camera of 114·6 mm diameter with Cu $K\alpha$ radiation. Specimen compositions were determined with an accuracy of ±0·8 at.% Pd for Au–Pd alloys, ±0·5 at.% Zn for Au–Zn alloys and ±0·5 ~ 1·0 at.% Mg for Ag–Mg alloys by referring to lattice parameter *vs* composition relations (Pearson, 1958; Maeland & Flanagan, 1964).

Thin foils suitable for electron diffraction were obtained by electropolishing after heat treatment. The electrolytes consisted of 25g CrO_3, 150cc HNO_3 and 200cc CH_3COOH for Au–Pd alloys (jet electropolishing), 100g saturated $CaCl_2$ solution, 73ml water, 4·5ml concentrated HCl, 25ml concentrated $HClO_4$ and 1g $CuNO_3$ for Au–Zn alloys, and 20% $HClO_4$ and 80% CH_3COOH for Ag–Mg alloys. A JEM 7A electron microscope was operated at 100 keV and diffraction patterns were obtained. Some diffraction patterns were observed by the use of the hot stage in the electron microscope.

III. Results

III. 1. Au–Pd *system*

Specimens of various compositions ranging from 22·8 to 91·2 at.% Pd were prepared. SRO diffuse scattering was detected in the specimens containing 28·2 to 61·6 at.% Pd. Typical diffraction patterns for the specimens containing 28·2, 40·6 and 50·8 at.% Pd with the incident beam parallel to the [001] axis are shown in Fig. 1 (*a*)–(*c*). The 28·2 at.% Pd alloy was annealed successively at 600 °C for 15 d, 400 °C for 40 d and then at 300 °C for 44 d, and the 40·6 and 50·8 at.% Pd alloys at 600 °C for 12 d and then at 400 °C for 72 d. Twofold and fourfold splittings of diffuse scattering are seen at 100, 110 and equivalent positions, bearing a close resemblance to those in the case of the Cu–Pd and Cu–Pt systems.

The separation m of the split diffuse maxima as defined in Fig. 1(*a*) was measured in terms of the distance between the 000 and 200 fundamental spots. It shows a monotonic increase with Pd content, as shown in Table 1. The value of m measured from the result of Lin *et al.* (1970) is also reproduced in Table 1.

Table 1. *Values of the separation, m, measured in terms of the distance between the* 000 *and* 200 *spots for* Au–Pd *alloys*

Composition x in $Au_{1-x}Pd_x$	Quenching temperature (°C)	m measured at quenched state	m measured by Lin *et al.* (1970)
0·282	300	0·15 ± 0·01	
0·338	400	0·17 ± 0·01	
0·40*			0·25
0·406	400	0·22 ± 0·01	
0·508	400	0·27 ± 0·01	
0·616	300	0·34 ± 0·015	

* This is the nominal composition of the sample. However, the lattice parameter measured by Lin *et al.* (1970) corresponds to that of the Au–44·0 at.% Pd alloy. [Refer to the lattice parameter *vs* composition relation (Maeland & Flanagan, 1964).]

Another important feature is the peculiar shape of the diffuse scattering which consists of four weak diffuse streaks around 110 and its equivalent positions. The positions of the fourfold split diffuse maxima correspond to the intersections of these streaks. The streaks were not observed on the distribution of X-ray diffuse scattering for the 40·0 at.% Pd alloy (Lin *et al.*, 1970). This difference may be due to the lack of angular resolution involved in the X-ray counter spectrometer method.

III. 2. Au–Zn *system*

Although specimens with compositions ranging from 6·6 to 29·0 at.% Zn were examined, the SRO diffuse scattering was observed only in the composition range of 6·6 to 24·2 at.% Zn. Typical diffraction patterns for specimens containing 6·6 and 22·0 at.% Zn with the incident beam parallel to the [001] axis are shown in Fig. 2(*a*) and (*b*). The 6·6 at.% Zn alloy was annealed at 500 °C for 1 d and then at 400 °C for 4 d, and the 22·0 at.% Zn alloy at 500 °C for 5 d, prior to quenching. In the alloys of Zn content greater than about 20 at.%, the ordering turned out to be a very quick process, so that the short-range-ordered state could not be retained by quenching. Therefore, diffraction patterns for such alloys were observed by the use of the hot stage of the electron microscope at high temperatures ($> T_c$).

Twofold and fourfold splittings of diffuse scattering are shown at 100, 110 and equivalent positions. The separation m increases monotonically with Zn content, as seen in Table 2. The diffuse scattering at 110 and its equivalent positions consists of four weak diffuse streaks with a slight curvature as shown in Fig. 8 of part I. The positions of the fourfold split maxima correspond to the intersections of these streaks.

III. 3. Ag–Mg *system*

Specimens of compositions ranging from 9·1 to

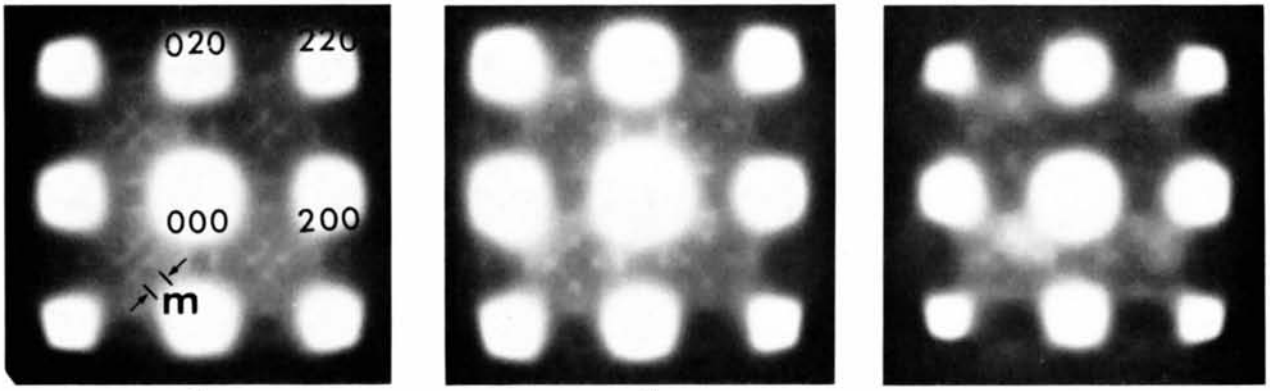

(*a*) (*b*) (*c*)

Fig. 1. Electron diffraction patterns of disordered Au–Pd alloys. Incident beam is parallel to [001] of the fundamental lattice. (*a*) 28·2 at.% Pd, (*b*) 40·6 at.% Pd, (*c*) 50·8 at.% Pd. Indices refer to the fundamental lattice.

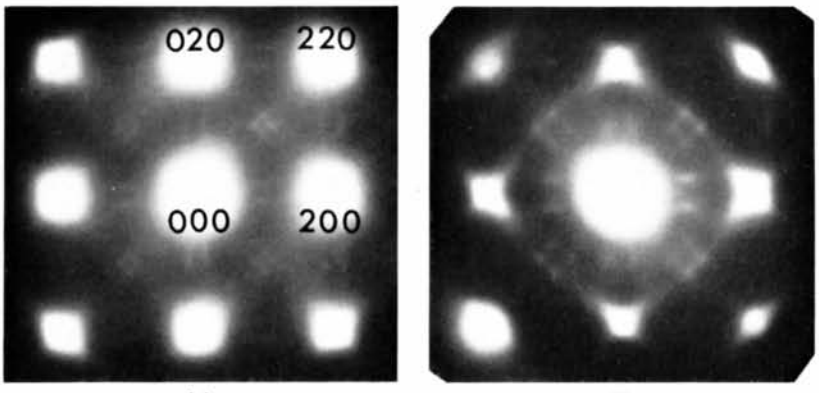

(*a*) (*b*)

Fig. 2. Diffraction patterns of disordered Au–Zn alloys. (*a*) 6·6 at.% Zn, (*b*) 22·0 at.% Zn. [001] incidence.

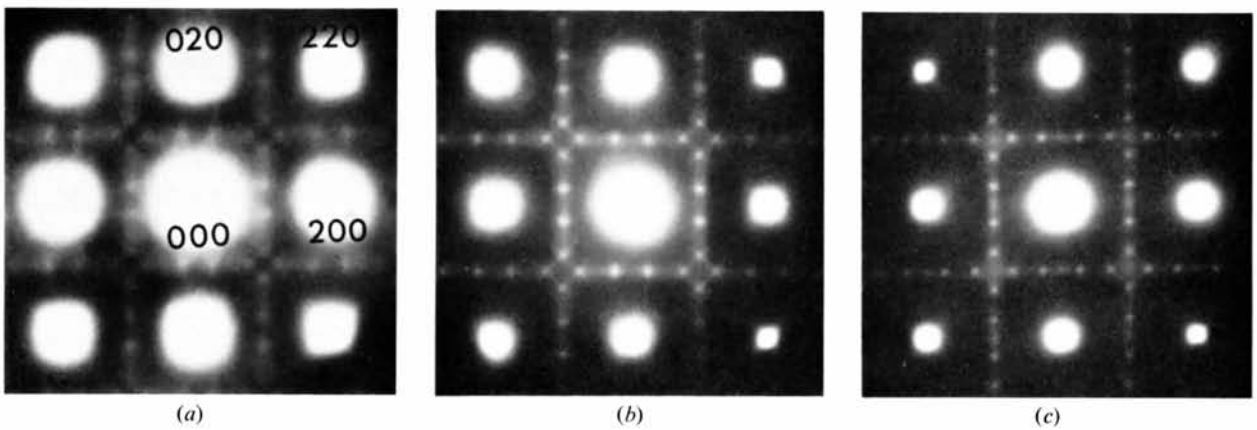

(*a*) (*b*) (*c*)

Fig. 3. Diffraction patterns of disordered Ag–Mg alloys. (*a*) 16·7 at.% Mg, (*b*) 19·0 at.% Mg, (*c*) 24·2 at.% Mg. [001] incidence.

[*To face p.* 785

Table 2. *Values of the separation, m, measured in terms of the distance between the* 000 *and* 200 *spots for* Au–Zn *alloys*

Composition x in $Au_{1-x}Zn_x$	Quenching temperature (°C)	m measured at quenched state	m measured at $T(>T_c)$
0·066	400	0·098±0·007	
0·100	300	0·115±0·005	
0·151	500	0·130±0·005	
0·170	500	0·138±0·005	
0·220			0·163±0·005
0·242			0·176±0·005

27·6 at.% Mg were examined, and SRO diffuse scattering was observed in the composition range from 10·8 to 27·6 at.% Mg. Typical diffraction patterns for the specimens containing 16·7, 19·0 and 24·2 at.% Mg with the incident beam parallel to the [001] axis are shown in Fig. 3(*a*)–(*c*). The alloys were annealed at 500 °C for 5 d and quenched into ice brine. Twofold and fourfold splittings of diffuse scattering are seen at 100, 110 and equivalent positions, bearing a resemblance to those of the Au–Pd and Au–Zn alloys, and the separation m increases with Mg content as shown in Table 3.

Table 3. *Values of the separation, m, measured in terms of the distance between the* 000 *and* 200 *spots for* Ag–Mg *alloys*

Composition x in $Ag_{1-x}Mg_x$	Quenching temperature (°C)	m measured at quenched state
0·108	300	0·126±0·011
0·157	300	0·152±0·005
0·167	500	0·157±0·005
0·190	500	0·174±0·005
0·229	500	0·191±0·005
0·242	500	0·197±0·005
0·272	500	0·204±0·005
0·276	500	0·211±0·005

However, the intensity distribution of diffuse scattering for this alloy system is somewhat different from that for the Au alloys. That is, additional diffuse streaks parallel to the h and k axes are observed through $h10$, $h30$, ... and $1k0$, $3k0$, ... positions respectively.

It is known that the half period M of the ordered one-dimensional anti-phase domain structure is 2·0 for the alloys with Mg less than about 22 at.% and decreases gradually to 1·7 as the Mg content increases from 22 at.% (Schubert *et al.*, 1955; Fujiwara *et al.*, 1958; Hanhi *et al.*, 1971). In the present study, after the SRO diffuse scattering was examined, the specimens of compositions ranging from 19·0 to 27·6 at.% Mg were annealed at temperatures below T_c to attain the ordered state, and the values of M were measured. The results were consistent with those of Fujiwara *et al.* (1958) and Hanhi *et al.* (1971). This means that the alloy composition has been preserved even after a long period of annealing in an argon atmosphere.

IV. Discussion

In part I, it was shown in detail that the SRO diffuse scattering reflects the form of the Fermi surface *via* the shape of $V(\mathbf{k})$, the Fourier transform of the atomic-pair interaction potential. For a flat portion of the Fermi surface, there is a logarithmic singularity in $V(\mathbf{k})$ itself at $\mathbf{k}=2\mathbf{k}_F\pm\mathbf{g}$ ($\mathbf{k}_F$=Fermi wave vector, $\mathbf{g}$=reciprocal lattice vector), where a pronounced minimum in $V(\mathbf{k})$ may appear, and a maximum in the diffuse-scattering intensity may correspondingly appear in reciprocal space.

The present experiment proved that the separation of the split diffuse maxima changes with alloy composition x for the Au–Pd, Au–Zn and Ag–Mg systems and that the diffuse scattering at 110 and its equivalent positions consists of four weak diffuse streaks. It can

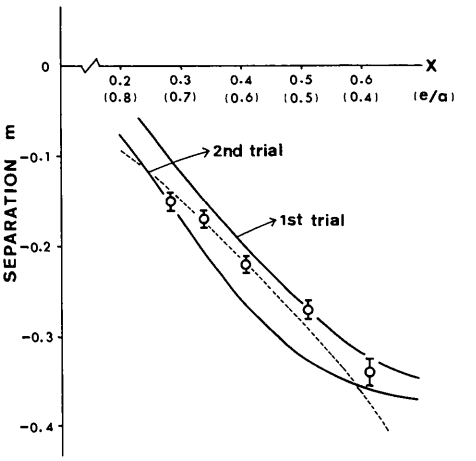

Fig. 4. Measured values of the separation, m, *vs* composition, x, of the Au–Pd system. The dotted curve shows the relation calculated from (1) for $t=0{\cdot}91$. The solid curves were obtained with the rigid-band model.

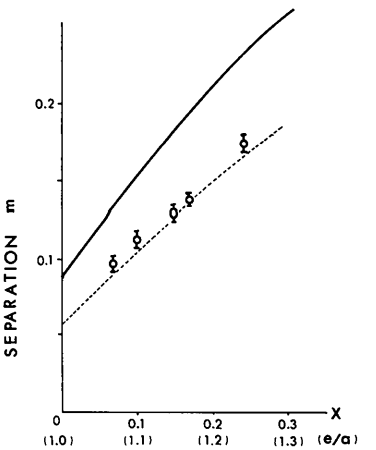

Fig. 5. Measured values of the separation, m, *vs* composition, x, of the Au–Zn system. The dotted curve shows the relation calculated from (1) for $t=0{\cdot}945$. The solid curve was obtained with the rigid-band model.

be concluded, therefore, that the Fermi surface of disordered Au–Pd, Au–Zn and Ag–Mg alloys has flat regions normal to the [110] directions resembling the form of the Fermi surface of Au and Ag (Roaf, 1962), and $\mathbf{k}_F^{110}$, the Fermi wave vector parallel to the [110] directions, monotonically decreases with increasing Pd content and increases with Zn and Mg content.

Using the nearly-free-electron model as previously discussed in part I, a relation between m and the electron–atom ratio (e/a) is given as

$$m=\left[\frac{12}{\pi}(e/a)\right]^{1/3} t-1/2\,, \qquad (1)$$

where t is a truncation factor which gives a measure of the non-sphericity of the Fermi surface, defined in Fig. 9 of part I. The dotted curves in Figs. 4, 5 and 6 were obtained from (1), assuming the number of conduction electrons to be zero for Pd, one for Au and Ag and two for Zn and Mg. The values of t for the three curves are 0·91, 0·945 and 0·955. Non-sphericity of the Fermi surface in the [110] directions has been calculated by Roaf (1962) to be 0·945 for Au and 0·965 for Ag. The t value obtained for the disordered Au–Zn system in the present analysis agrees with that of pure Au, but the values for Au–Pd and Ag–Mg systems are slightly smaller than those of pure Au and Ag.

With the nearly-free-electron model, it is possible to obtain curves for the relation between m and (e/a) which fit the experimental data, by using the t value as an adjustable parameter, as shown above. It must be noted, however, that the (e/a) values assumed in the analysis can be another important adjustable parameter. As a better model than the nearly-free-electron, the rigid-band model was then adopted in the analysis.

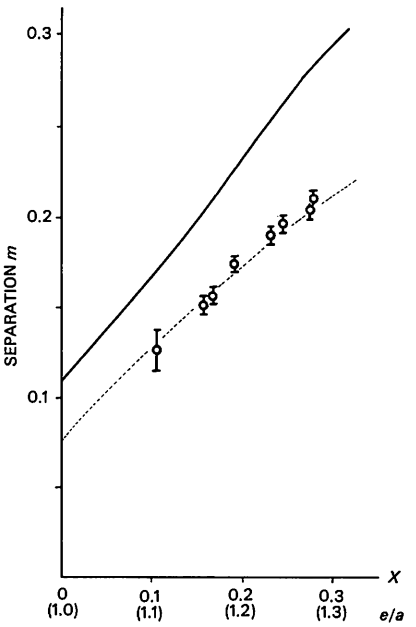

Fig. 6. Measured values of the separation, m, *vs* composition, x, of the Ag–Mg system. The dotted curve shows the relation calculated from (1) for $t=0{\cdot}955$. The solid curve was obtained using the rigid-band model.

For the Au–Pd system, the energy bands of Au and Pd calculated by Christensen & Seraphin (1971) and Mueller, Freeman, Dimmock & Furdyna (1970), respectively, were used, and the following two calculations were performed.

The first trial. The atomic configurations of Au and Pd are $5d^{10}6s^1$ and $4d^{10}5s^0$, with 11 and 10 conduction electrons respectively. Since the band structure of Pd is similar to that of Au, the energy level filled with 10 electrons in the density of states $N(E)$ *vs* energy curve of Au was assumed to be the virtual Fermi energy of Pd, E_F^{virt} (Pd), and the Fermi energy $E_F(x)$ at the composition x was determined so as to satisfy the relations

$$x=\int_{E_F^{virt}(\mathrm{Pd})}^{E_F(x)} N(E)\mathrm{d}E\,, \quad 1=\int_{E_F^{virt}(\mathrm{Pd})}^{E_F(\mathrm{Au})} N(E)\mathrm{d}E\,. \qquad (2)$$

Then, the Fermi wave vector $\mathbf{k}_F^{110}(x)$ was obtained from the E *vs* $\mathbf{k}$ curve of Au. The separation m deduced from this calculation is shown in Fig. 4 by the solid curve (1st trial).

The second trial. The value of E_F^{virt}(Pd) was obtained from the E *vs* $\mathbf{k}$ curve of Au so that the corresponding Fermi wave vectors along the specific axes coincide with the Fermi wave vectors of Pd calculated by Mueller *et al.* (1970), and $E_F(x)$ was determined so as to satisfy (2). Then, $\mathbf{k}_F^{110}(x)$ was obtained in the same way as in the first trial. The result is also shown in Fig. 4 by the solid curve (2nd trial).

The calculated m *vs* x curves agree qualitatively with the experimental result, although it cannot be said whether the first or the second trial is better. The calculated separation m does not change very much for compositions greater than about 60 at.% Pd (for the first trial) or 50 at.% Pd (for the second trial), because the d-like electrons start to contribute to the Fermi energy level.

For the Au–Zn and Ag–Mg systems, calculation by the second trial can not be performed, because Zn and Mg have a h.c.p. structure. Using the energy bands of Au and Ag calculated by Christensen & Seraphin (1971) and Christensen (1972), respectively, the m *vs* x curves were obtained with the first trial, as shown in Figs. 5 and 6 by solid curves. The agreement with the experimental results is not good, however, in these cases.

The rigid band model was also applied to the experimental results for disordered Cu–Pd and Cu–Pt alloys reported in part I. Data for the energy band of Cu calculated by Burdick (1963) (E *vs* $\mathbf{k}$) and Faulkner, Davis & Joy (1967) [$N(E)$ *vs* E] were used. The m *vs* composition curve obtained from the first trial is shown in Fig. 7. The agreement between the calculation and experimental results is very good.

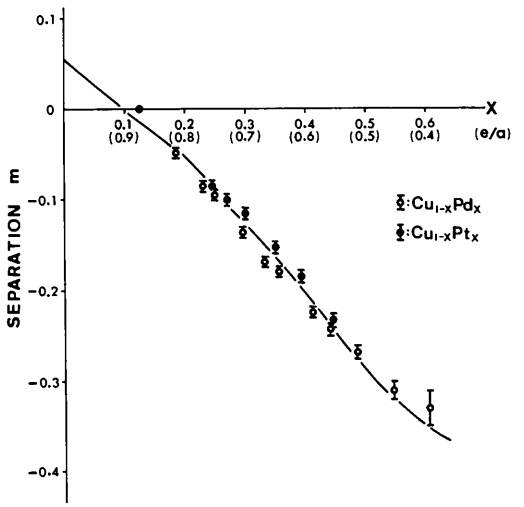

Fig. 7. Measured values of the separation, m, *vs* composition, x, of the Cu–Pd and Cu–Pt systems. The solid curve was obtained with the rigid-band model.

It should be emphasized that the change of $\mathbf{k}_F^{110}$ with composition observed through the SRO diffuse scattering in the Au–Pd, Cu–Pd and Cu–Pt systems is explained reasonably well with the rigid band model. However, the agreement is poor for the alloys containing Zn or Mg. It seems that a theoretical calculation of the Fermi surface is needed to obtain an agreement for these alloys.

The result of the present analysis supports the Fermi-surface-imaging concept proposed by Krivoglaz (1969), and is consistent with the conclusions reported so far that the composition-dependent SRO diffuse maxima originate from the long-range electronic energy terms and that the higher-order atomic-pair interaction potentials play an important role in the characteristic features of diffuse scattering (Ohshima & Watanabe, 1973; Ohshima, Watanabe & Harada, 1976). However, the additional diffuse streaks, which pass through the $h10, h30, \ldots$ and $1k0, 3k0, \ldots$ positions and are parallel to the h and k axes, respectively, observed from the Ag–Mg alloys in the present study are scarcely composition dependent. Using the linearized approximation for the correlation functions of a binary alloy by Clapp & Moss (1968), such diffuse scattering can be reproduced if only the first nearest neighbour atomic-pair interaction potential $V_1(>0)$ is considered. It may be concluded, therefore, that the additional diffuse streaks originate from the short-range ion-core repulsive force, and that the diffuse scattering observed from the Ag–Mg alloys is the superposition of these streaks and the composition-dependent diffuse scattering originating from the long-range electronic interactions.

The authors wish to thank to Dr Takemi Yamada for helpful discussion. This work was partly supported by the Grant-in-Aid for Fundamental Scientific Research from the Ministry of Education.

References

BURDICK, G. A. (1963). *Phys. Rev.* **129**, 138–150.

CHRISTENSEN, N. E. (1972). *Phys. Stat. Sol. (b)*, **54**, 551–563.

CHRISTENSEN, N. E. & SERAPHIN, B. O. (1971). *Phys. Rev. (B)*, **4**, 3321–3344.

CLAPP, P. C. & MOSS, S. C. (1968). *Phys. Rev.* **171**, 754–763.

COPELAND, W. D. & NICHOLSON, M. E. (1964). *Acta Metal.* **12**, 321–322.

COWLEY, J. M. & WILKINS, S. W. (1972). *Interatomic Potentials and Simulation of Lattice Defects*, pp. 265–280. New York: Plenum.

FAULKNER, J. S., DAVIS, H. L. & JOY, H. W. (1967). *Phys. Rev.* **161**, 656–664.

FUJIWARA, K., HIRABAYASHI, M., WATANABE, D. & OGAWA, S. (1958). *J. Phys. Soc. Japan*, **13**, 167–174.

HANHI, K., MÄKI, J. & PAALASSALO, P. (1971). *Acta Metal.* **19**, 15–20.

HANSEN, M. & ANDERKO, K. (1958). *Constitution of Binary Alloys*, 2nd ed. New York: McGraw-Hill.

HASHIMOTO, S. & OGAWA, S. (1970). *J. Phys. Soc. Japan*, **29**, 710–721.

IVERONOVA, V. I. & KATSNEL'SON, A. A. (1965). *Sov. Phys. Crystallogr.* **9**, 467.

IVERONOVA, V. I. & KATSNEL'SON, A. A. (1966). *Sov. Phys. Crystallogr.* **11**, 504–507.

IWASAKI, H. (1962). *J. Phys. Soc. Japan*, **17**, 1620–1633.

IWASAKI, H., HIRABAYASHI, M., WATANABE, D. & OGAWA, S. (1960). *J. Phys. Soc. Japan*, **15**, 1771–1783.

KAWASAKI, Y., INO, S. & OGAWA, S. (1971). *J. Phys. Soc. Japan*, **30**, 1758–1759.

KRIVOGLAZ, M. A. (1969). *Theory of X-ray and Thermal Neutron Scattering by Real Crystals*. New York: Plenum.

LIN, W., SPRUIEL, J. E. & WILLIAMS, R. O. (1970). *J. Appl. Cryst.* **3**, 297–305.

MAELAND, A. & FLANAGAN, T. B. (1964). *Canad. J. Phys.* **42**, 2364–2366.

MATSUO, Y., NAGASAWA, A. & KAKINOKI, J. (1966). *J. Phys. Soc. Japan*, **21**, 2633–2637.

MUELLER, F. M., FREEMAN, A. J., DIMMOCK, J. O. & FURDYNA, A. M. (1970). *Phys. Rev. (B)*, **1**, 4617–4635.

NAGASAWA, A., MATSUO, Y. & KAKINOKI, J. (1965). *J. Phys. Soc. Japan*, **20**, 1881–1885.

OHSHIMA, K. & WATANABE, D. (1973). *Acta Cryst.* A**29**, 520–526.

OHSHIMA, K., WATANABE, D. & HARADA, J. (1976). *Acta Cryst.* A**32**, 883–892.

PEARSON, W. B. (1958). *A Handbook of Lattice Spacings and Structures of Metals and Alloys*. Oxford: Pergamon Press.

RAETHER, H. (1952). *Angew. Phys.* **4**, 53–59.

ROAF, D. J. (1962). *Phil. Trans.* A**255**, 135–152.

SATO, K., WATANABE, D. & OGAWA, S. (1962). *J. Phys. Soc. Japan*, **17**, 1647–1651.

SCATTERGOOD, R. O., MOSS, S. C. & BEVER, M. B. (1970). *Acta Metal.* **18**, 1087–1098.

SCHUBERT, K., KIEFER, B., WILKENS, M. & HAUFLER, R. (1955). *Z. Metallkd.* **46**, 692–715.

WATANABE, D. (1959). *J. Phys. Soc. Japan*, **14**, 436–443.

WATANABE, D. & FISHER, P. M. J. (1965). *J. Phys. Soc. Japan*, **20**, 2170–2179.